PATHS FOR RURAL ECOLOGICAL RESTORATION AND ECOSYSTEM SERVICE ENHANCEMENT UNDER ECOLOGICAL AGRICULTURE: A REMOTE SENSING–DRIVEN SPATIOTEMPORAL MODELING AND MULTI-OBJECTIVE OPTIMIZATION STUDY

ZHOU, K. Q.

Fujian Agriculture and Forestry University, School of Landscape Architecture and Arts, Fuzhou, Fujian 350000, China
(e-mail: 13619638503@163.com)

(Received 16th Aug 2025; accepted 14th Nov 2025)

Abstract. In rural landscapes of northern China, high-intensity chemical inputs, fragmented land use, and poor ecological management have led to ecological degradation and a weakening of ecosystem services. This paper aims to improve environmental characteristics, soil quality, vegetation, and yields, reverse rural ecological degradation, enhance ecosystem services, and ensure sustainable agricultural development. To address these challenges, we integrated satellite remote sensing and unmanned aerial vehicle (UAV) multispectral imagery to assemble multi-dimensional, spatiotemporal ecological datasets, fused with environmental and agricultural management records. A deep spatiotemporal convolutional neural network (ST-CNN) has been created for fine-scale diagnostics and continuous assessments of soil quality, water status, and vegetation cover. From model outputs, we have implemented a multi-objective ecological-agriculture layout algorithm to jointly optimize (i) crop planting structure, (ii) on-farm biodiversity allocation, and (iii) water-fertilizer regulation strategies, explicitly balancing yield, resource use, and ecological benefits along the Pareto frontier. For a landscape case study, soil organic matter increased from 2.40% to 3.80%, the overall water quality index increased to a peak of 0.91, dissolved oxygen increased from 5.5 to 7.2 mg L^{-1}, and peak-season vegetation cover peaked at 86.0% in August, a change of 11.8 percentage points compared to unoptimized management. These results demonstrate that the combination of quantitative ecological monitoring with spatiotemporal deep learning and multi-objective optimization can result in quantifiable benefits in regulating and supporting ecosystem services without sacrificing productive functions under ecological agriculture. This workflow provides a transferable decision-making framework for precise restoration and service enhancement in rural regions with limited access to data.

Keywords: *ecological agriculture, rural ecological restoration, ecosystem services, quantitative ecology, remote sensing and UAV multispectral, spatiotemporal CNN, multi-objective optimization, biodiversity allocation, water–fertilizer management, landscape planning*

Introduction

Decades of agricultural expansion and high-intensity input regimes have degraded soils and water resources, reduced on-farm and landscape biodiversity, and increased pollution loads—largely due to excessive chemical inputs, irrational land use, and insufficient ecological management (Gu et al., 2023; Juncal et al., 2023; Madjar et al., 2024). These degradation processes erode multiple ecosystem services, including provisioning, regulating, supporting, and cultural services, thereby constraining sustainable rural development (Zhang et al., 2022; Morizet-Davis et al., 2023; Petrosillo et al., 2023). Advancing rural ecological restoration anchored in ecological (or agro-ecological) agriculture is therefore essential to improve environmental quality and to elevate ecosystem service provision, while simultaneously supporting rural revitalization

http://www.aloki.hu ● ISSN 1589 1623 (Print) ● ISSN1785 0037 (Online)
DOI: http://dx.doi.org/10.15666/aeer/2401_611633

and broader ecological-civilization goals (Wang et al., 2022; Knapp and Sciarretta, 2023; Yan et al., 2024).

However, rural ecological governance still faces three persistent limitations. First, environmental information systems struggle with cross-scale monitoring: spatial granularity and temporal revisit frequency are often traded off, updates are infrequent, and key processes are missed (Senf, 2022; Wang et al., 2024; Lenton et al., 2024; Gao, 2024; Lottering et al., 2025). Second, ecological assessments frequently rely on static or uni-dimensional indicators, which under-represent nonlinear interactions and time-varying feedbacks among soil, water, vegetation, and management drivers (Sutherland et al., 2022; Liu et al., 2023). Third, agricultural decision-making and restoration interventions are commonly empirical and poorly coupled with diagnostics, making it difficult to achieve quantitative, precise regulation at field-to-landscape scales (Zhai et al., 2022; Piczak et al., 2024).

Recent studies have improved individual components of this pipeline—e.g., remote-sensing classification of land cover, in situ testing of water and soil physico-chemical parameters, machine-learning prediction of environmental factors, and land-use optimization under ecological red-line or conservation constraints (Mehmood et al., 2022; Kaur et al., 2022; Lewandowski et al., 2023). Yet important gaps remain: (i) robust spatiotemporal integration of multi-source ecological and agricultural data; (ii) co-optimization of ecological and production objectives rather than single-criterion planning; and (iii) an adaptive, closed-loop that links data acquisition, diagnostic assessment, and operational configuration. Without these, restoration outcomes and ecosystem-service gains remain limited and difficult to generalize (Pfeifer et al., 2023; Maes et al., 2024; Bai et al., 2025).

Addressing the core gap in existing research's failure to construct a closed-loop system encompassing multi-source data fusion, spatiotemporal dynamic diagnosis, and multi-objective collaborative optimization, this paper proposes an ecological agriculture-driven rural ecological restoration pathway to fill this gap by integrating monitoring, assessment, and optimization modules. First, this paper integrates satellite remote sensing and UAV multispectral imagery, combined with ground-based soil and water monitoring data and agricultural management records, to construct a high spatiotemporal resolution ecological environment dataset, resolving the issues of insufficient cross-sensor and cross-scale data integration and inadequate spatiotemporal continuity. Second, a deep spatiotemporal convolutional neural network (ST-CNN) for multi-scale feature extraction is developed to achieve dynamic diagnosis of soil quality, water status, and vegetation cover, overcoming the limitations of static or single-dimensional ecological assessments in characterizing nonlinear interactions and temporal feedback. Finally, a multi-objective optimization framework based on the Pareto front is constructed to simultaneously optimize crop planting structure, farmland biodiversity allocation, and refined water and fertilizer regulation strategies, and an iterative feedback mechanism is introduced to update management plans based on new observation data, forming an adaptive closed loop of "data acquisition-diagnosis and assessment-operational configuration." This provides a scalable and transferable decision-making framework for building sustainable rural ecosystems.

This work contributes: (1) a cross-sensor, cross-scale data-fusion pipeline tailored to rural ecological monitoring; (2) an interpretable ST-CNN for fine-scale, time-varying ecological diagnostics; (3) a Pareto-based, multi-objective co-optimization of production and ecological targets, explicitly incorporating biodiversity and water–nutrient

http://www.aloki.hu ● ISSN 1589 1623 (Print) ● ISSN1785 0037 (Online)
DOI: http://dx.doi.org/10.15666/aeer/2401_611633

management; and (4) an operational feedback architecture that links monitoring and assessment to actionable restoration decisions.

Related work

Restoration pathways within ecological agriculture

Existing research on rural ecological restoration has primarily focused on soil enhancement, water-environment management, and the optimization of agricultural practices. Using a PRISMA-guided (Preferred Reporting Items for Systematic Reviews and Meta-Analyses) methodology, Colombi et al. (2025) conducted a systematic review and quantitative synthesis, reporting that regenerative organic agriculture (ROAg) generally improves soil health and ecosystem services. Although grain yields are often lower than those under conventional management, ROAg tends to deliver higher plant nutrient density, underscoring the potential of rebalancing production goals with nutritional and ecological outcomes.

To mitigate non-point source pollution, Bai et al. (2025) integrated 115 datasets and performed detailed analyses using generalized additive models (GAMs) to identify the key drivers of nutrient removal in ecological ditches. Their findings revealed that plant assemblages, ditch lining, temperature, and hydraulic retention time are critical for the removal of total nitrogen and total phosphorus, leading to management recommendations aimed at reducing eutrophication risks in agricultural landscapes.

Kabir et al. (2023) analyzed the role of biochar and synthesized recent advances demonstrating its multiple functions in enhancing soil physicochemical properties, improving fertility and water-use efficiency, and removing pollutants. These findings further reinforce biochar's potential as a sustainable strategy for promoting soil health, supporting agricultural productivity, and contributing to climate-change mitigation.

However, these studies mostly focus on the local effects of single restoration technologies, lacking in-depth exploration of the inherent trade-off mechanism between output and environmental benefits, and failing to clearly explain the balance path between the two. At the same time, the existing results lack cross-regional applicability, do not fully consider the differences in conditions in different regions, and lack research on integrating multiple restoration technologies into an operable and adaptive complete workflow, making it difficult to support large-scale and precise rural ecological restoration practices.

Monitoring and evaluation of ecosystem service improvements

To strengthen monitoring and decision support, scholars increasingly combine multi-source data with multi-dimensional assessment frameworks. Schwantes et al. (2023) operationalized the EESV framework proposed by GEO BON in three case studies from British Columbia (Canada), using trend and intervention analyses to reveal changes in ecosystem-service variables and policy effects. They also outlined challenges, potential solutions, and quantitative guidance, demonstrating the framework's value for indicator harmonization and policy-relevant assessment. In addition to framework initiatives complemented by technical advancements, Masenyama et al. (2022) conducted a systematic review of 222 studies that quantified ecosystem services in grassland ecosystems utilizing remote sensing technology, while drawing out geographical and sensor publishing- related patterns. Their study identified biomass, canopy water storage

http://www.aloki.hu ● ISSN 1589 1623 (Print) ● ISSN1785 0037 (Online)
DOI: http://dx.doi.org/10.15666/aeer/2401_611633

capacity, and leaf area index as elements of significance for recognizing water-related services. Building off of indicator development, and tooling, Selsam et al. (2024) introduced the ESIS/Imalys platform, which aims to facilitate both remote-sensed processing and ecosystem property data indicators scalability, using both raster and vector formats. Examples of applications existed, assessing landscape diversity, land-use-intensity/extent, and other related metrics, and promoting an open approach to access post-processing ecosystem indicators at the global scale. Singh and Gaurav (2023) conducted an empirical study using imagery and deep learning fusion for surface soil moisture estimation, demonstrating an effective mapping between image features and soil variables. Song et al. (2023) used UAV hyperspectral data for spatial prediction and mapping of soil texture, illustrating the high-precision advantages of hyperspectral data in soil property characterization.

Despite these advances, challenges remain. Firstly, cross-regional validation efforts are limited, and the universality and applicability of existing findings need further verification. Secondly, multi-source data integration is insufficient, lacking the ability to capture the spatiotemporal continuity of ecosystems and failing to comprehensively reflect the dynamic changes in ecological processes. Furthermore, the lack of a long-term dynamic monitoring process that directly links monitoring and diagnosis with management decisions prevents the formation of a closed loop of monitoring-assessment-decision, hindering the effective transformation of monitoring results into targeted ecological restoration action plans.

Research gap and positioning

In sum, prior work has advanced restoration practices and ecosystem-service monitoring, but falls short of delivering a closed-loop system that (a) fuses satellite and UAV observations into high-temporal-resolution datasets, (b) performs interpretable, spatiotemporal diagnostics of soil–water–vegetation dynamics, and (c) executes multi-objective co-optimization that makes the yield–environment trade-off explicit and actionable. Our study addresses these needs by integrating monitoring–assessment–optimization within a single, adaptive workflow, thereby enabling precise restoration and ecosystem-service enhancement under ecological agriculture.

Materials and methods

Data collection and preprocessing

To achieve refined restoration of the rural ecological environment and enhance ecosystem services, this study integrated multi-source, multi-temporal, and multi-scale ecological and environmental information during the data collection phase. Data sources included drone multispectral imaging, satellite remote sensing observations, ground-based soil and water quality monitoring point measurements, and agricultural production management records. These multi-source data differed in spatial resolution, temporal resolution, and spectral information. To ensure the accuracy of subsequent analysis, high-precision spatiotemporal registration and quality control were required before data processing. UAV multispectral imagery was calibrated during acquisition using high-precision GNSS and inertial navigation systems. Radiometric calibration and atmospheric correction were performed after acquisition to eliminate sensor response variations and atmospheric scattering effects. Satellite remote sensing data was post-acquisition using

http://www.aloki.hu ● ISSN 1589 1623 (Print) ● ISSN1785 0037 (Online)
DOI: http://dx.doi.org/10.15666/aeer/2401_611633

high-order polynomial geometric correction and terrain correction methods to reduce spatial distortion caused by terrain undulation and sensor observation angles. Ground monitoring data was processed before input into the system, including outlier removal and missing value interpolation, to ensure statistical consistency and stability across all data sources.

In order to achieve the fusion processing of different data sources, this study performs spatial gridding operations on multispectral images and measured data, projecting all data into a unified coordinate system and grid resolution. Spatial interpolation uses the Inverse Distance Weighting (IDW) method, and its calculation formula is:

$$V(x_0)=\frac{\sum_{i=1}^{n}\frac{V_i}{d_i^p}}{\sum_{i=1}^{n}\frac{1}{d_i^p}} \quad \text{(Eq.1)}$$

Here, $V(x_0)$ represents x_0 the attribute value at the location to be interpolated, V_i represents x_i the observed value at the known location, d_i represents x_0 the distance between and , p and $x_i$is the distance decay exponent. In this study, p is set to 2 to enhance the influence of neighboring points on the interpolation results. This interpolation method ensures spatial continuity between the image spectral information and the point monitoring data, providing a consistent input data format for subsequent ST-CNN modeling.

The data collection characteristics of this section are shown in *Table 1*. The table lists the spatial resolution, temporal resolution, band range, acquisition period of various data sources and their main uses in the method system, providing a clear parameter basis for the subsequent modeling input definition.

Table 1. *Data collection sources and characteristics*

Data Type	Spatial Resolution	Temporal Resolution	Spectral Range (nm)	Collection Cycle	Main Use
UAV Multispectral	0.1 m	7 days	450–900	Continuous	Vegetation cover & health
Satellite Remote Sensing	10 m	16 days	400–2500	Long-term	Soil moisture & vegetation index
Soil Monitoring Points	Point	Quarterly	N/A	Regular	Organic matter & nutrients
Water Quality Points	Point	Monthly	N/A	Regular	Water quality index
Agricultural Records	N/A	Annual	N/A	Annual	Crop types & tillage

After data fusion, the noisy areas of the multispectral imagery were masked using a Spectral Angle Mapper (SAM) classification mask. This removed clouds, shadows, and non-target areas, thereby retaining valid observation pixels within the study area. This process ensured the spectral consistency of the input data and reduced the interference of invalid information on model training. After preprocessing, the data was fed into the ST-CNN model input layer through a unified data interface, forming a multidimensional spatiotemporal input matrix of soil quality, water quality, and vegetation cover. Its structure is shown in *Figure 1*.

http://www.aloki.hu ● ISSN 1589 1623 (Print) ● ISSN1785 0037 (Online)
DOI: http://dx.doi.org/10.15666/aeer/2401_611633

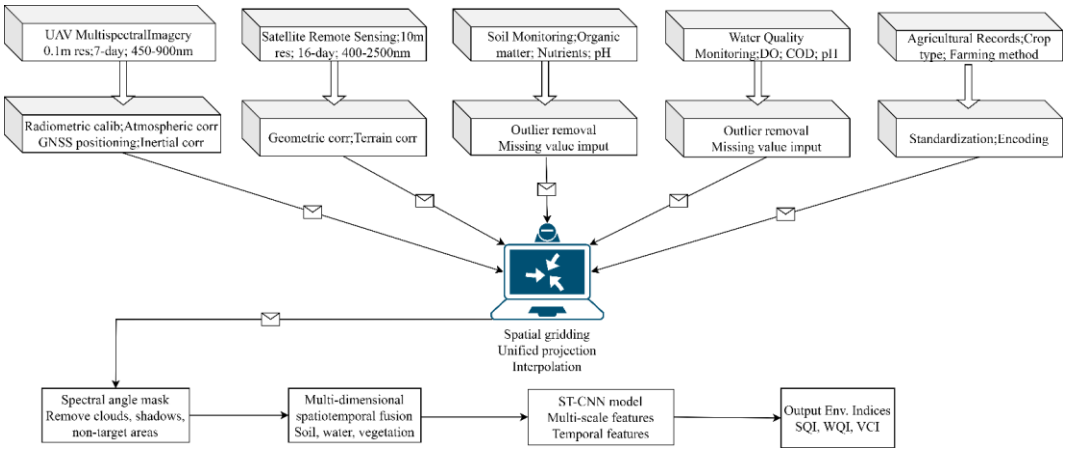

Figure 1. *Data flow and innovation structure*

ST-CNN environmental diagnosis module

To achieve refined identification of the multidimensional characteristics of the rural ecological environment and characterize its dynamic trends, this study constructed an ST-CNN environmental diagnosis module. This module takes the high-spatiotemporal resolution, multi-dimensional noise-suppressed ecological and environmental dataset produced in Section 3.1 as input and extracts environmental features using a combination of spatial and temporal convolution. The spatial convolution component extracts the spatial structural features of soil, water, and vegetation in the two-dimensional domain using multi-scale convolution kernels, enhancing the ability to capture both local and global features at different resolutions. The temporal convolution component uses one-dimensional convolution in the time domain to capture the changing trends of environmental features at different time scales, thereby obtaining information on the dynamic evolution of environmental quality. A weighted residual connection structure is introduced in the feature fusion stage to mitigate the risk of vanishing gradients and maintain the integrity of the original information. Ultimately, the module outputs time-series predictions for the Soil Quality Index (SQI), Water Quality Index (WQI), and Vegetation Coverage Index (VCI).

In terms of index calculation, the SQI is based on the weighted and normalized comprehensive results of soil organic matter, pH value, and nutrient content. The WQI is calculated by weighting and normalizing water transparency, dissolved oxygen, nitrogen and phosphorus concentrations, etc., and the VCI is obtained by linearly transforming the time series data of the Normalized Difference Vegetation Index (NDVI). The unified calculation model of the three types of indicators can be expressed as:

$$I_c = \sum_{k=1}^{n} w_k \cdot \frac{X_k - X_k^{min}}{X_k^{max} - X_k^{min}} \quad \text{(Eq.2)}$$

where I_c represents the comprehensive index value (SQI for soil quality, WQI for water quality, and VCI for vegetation), X_k is k the observed value of the environmental parameter, X_k^{min} and are X_k^{max} the minimum and maximum values of the parameter, respectively, w_k is the weight coefficient for each parameter in the comprehensive evaluation, n and is the total number of parameters involved in the calculation. This

http://www.aloki.hu ● ISSN 1589 1623 (Print) ● ISSN1785 0037 (Online)
DOI: http://dx.doi.org/10.15666/aeer/2401_611633

calculation method ensures the comparability and stability of each indicator in the comprehensive evaluation by normalizing data from different sources and dimensions, and reflects the importance of the parameter in the target evaluation through weight assignment.

The ST-CNN architecture consists of an input layer, a multi-scale spatial convolution layer, a temporal convolution layer, a feature fusion and residual connection layer, and a multi-task output layer. Feature extraction and prediction for soil, water, and vegetation are performed concurrently within the same model framework, reducing model training time and improving feature sharing efficiency. The multi-scale spatial convolution kernels in the network are designed to have kernel sizes of [3×3], [5×5], and [7×7] to accommodate spatial feature distributions at different scales. The temporal convolution layer uses dilated convolution to expand the receptive field and improve the accuracy of capturing long-term trends. The model architecture and its key components are shown in *Figure 2*.

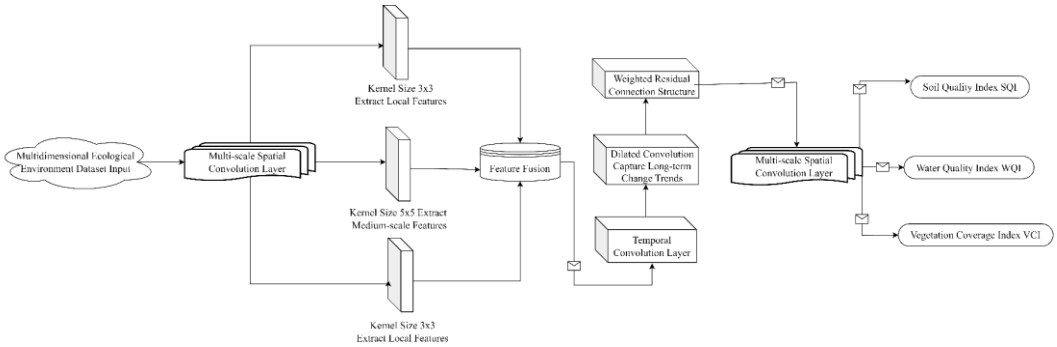

Figure 2. *Schematic diagram of the ST-CNN environmental diagnosis model structure*

The calculation parameters for environmental quality diagnostic indicators vary among different environmental factors. The parameter selection, data sources, and weightings for each indicator were determined based on historical data from the experimental area and expert scoring. For soil quality parameters, organic matter content was weighted at 0.4, pH at 0.3, and nutrient content at 0.3. For the comprehensive water quality index, dissolved oxygen was weighted at 0.35, nitrogen concentration at 0.25, phosphorus concentration at 0.25, and transparency at 0.15. For vegetation cover calculations, the annual mean NDVI was weighted at 0.6, and seasonal variation was weighted at 0.4. The relevant parameters and data sources are shown in *Table 2*.

Multi-objective optimization of ecological agriculture layout module

The multi-objective optimization ecological agricultural layout module takes environmental quality diagnosis results and agricultural production constraints as inputs, and constructs an optimization model that simultaneously meets multiple ecological and agricultural objectives under spatial constraints and resource utilization restrictions. The model takes maximizing the comprehensive score of ecosystem service functions, minimizing environmental risks, and maximizing agricultural output stability as optimization objectives, and defines the decision variables as plot-level crop planting structure configuration vectors $\mathbf{x}=(x_1,x_2,\ldots,x_n)$, x_i where i The crop type of each plot is coded, and the biodiversity configuration variable is introduced $\mathbf{b}=(b_1,b_2,\ldots,b_n)$ to

http://www.aloki.hu ● ISSN 1589 1623 (Print) ● ISSN1785 0037 (Online)
DOI: http://dx.doi.org/10.15666/aeer/2401_611633

represent the habitat type combination of the plot, and the water and fertilizer control parameter vector $\mathbf{w}=(w_1,w_2,\ldots,w_m)$ represents the irrigation and fertilization amount of each control unit. In the optimization objective function, the comprehensive score of ecosystem service function $F_{\text{eco}}(\mathbf{x},\mathbf{b},\mathbf{w})$ is composed of the weighted sum of supply service, regulation service, support service and cultural service, as shown in the formula:

$$maxF_{\text{eco}}(\mathbf{x},\mathbf{b},\mathbf{w})=\sum_{k=1}^{K}\ \alpha_k S_k(\mathbf{x},\mathbf{b},\mathbf{w}) \quad \text{(Eq.3)}$$

where is the scoring function S_k for k the ecosystem service type, α_k and is the corresponding weight. The weight value is determined by the sensitivity analysis results of multi-source monitoring data and satisfies the following conditions $\sum_{k=1}^{K}\ \alpha_k=1$: The environmental risk function $F_{\text{risk}}(\mathbf{x},\mathbf{b},\mathbf{w})$ is calculated based on the risk of nitrogen and phosphorus loss, water resource consumption intensity, and soil degradation probability, as shown in the formula:

$$minF_{\text{risk}}(\mathbf{x},\mathbf{b},\mathbf{w})=\beta_1 R_{\text{np}}(\mathbf{x},\mathbf{w})+\beta_2 R_{\text{water}}(\mathbf{x},\mathbf{w})+\beta_3 R_{\text{soil}}(\mathbf{x}) \quad \text{(Eq.4)}$$

Among them, R_{np} represents the nitrogen and phosphorus loss risk index, R_{water} represents the water resource consumption intensity, R_{soil} and represents the probability of soil degradation β_1 . β_2 , β_3. The agricultural output stability $F_{\text{prod}}(\mathbf{x})$ takes the inverse of the multi-year yield variance as the target value, as shown in the formula:

$$maxF_{\text{prod}}(\mathbf{x})=\frac{1}{\sigma_Y^2(\mathbf{x})} \quad \text{(Eq.5)}$$

Among them, $\sigma_Y^2(\mathbf{x})$ represents the variance of crop yields in different plots under different climate scenarios. Combining the above three objectives, a multi-objective optimization problem is established:

$$maxF(x,b,w)=(Feco(x,b,w),-Frisk(x,b,w),Fprod(x)) \quad \text{(Eq.6)}$$

The constraints include plot area restrictions $\sum_{i\in C_j}\ a_i\leq A_j$, crop rotation cycle constraints $x_i\neq x_i^{t-1}$ (where t represents the year), and total water and fertilizer resource restrictions $\sum_{l=1}^{m}\ w_l\leq W_{\max}$ and $\sum_{l=1}^{m}\ f_l\leq F_{\max}$, where a_i represents i the area of the th plot, is the upper limit of the available area of A_j the th j type of land, w_l and f_l are the irrigation and fertilization amounts, respectively.

To solve this multi-objective optimization problem, an improved genetic algorithm (GA) performs a global search. The population encoding **x**, **b**, **w** represents the joint representation as a chromosome, and the fitness function scalarizes the multiple objectives based on the weighted Tchebycheff decomposition method. The crossover operation uses piecewise uniform crossover to ensure the combinatorial diversity of crop types and biodiversity configurations. The mutation operation introduces an adaptive mutation probability adjustment mechanism based on environmental sensitivity to improve search accuracy in high-risk areas. The algorithm utilizes an elite retention strategy during the iteration process to prevent the loss of optimal solutions. A spatial proximity constraint correction scheme is introduced to ensure that the optimization results form a geographically contiguous ecological agricultural layout. The final output

http://www.aloki.hu ● ISSN 1589 1623 (Print) ● ISSN1785 0037 (Online)
DOI: http://dx.doi.org/10.15666/aeer/2401_611633

solution vector is mapped to plot-level crop planting structure, biodiversity configuration plan, and water and fertilizer control parameters, which serve as the basis for subsequent restoration and improvement paths.

Table 2. *Calculation parameters of environmental quality diagnostic indicators*

Index Category	Parameter Name	Weight	Data Source
Soil Quality Index (SQI)	Organic Matter Content	0.40	In-situ measurements from soil monitoring sites
	pH Value	0.30	In-situ measurements from soil monitoring sites
	Nutrient Content (Integrated)	0.30	In-situ measurements from soil monitoring sites
Water Quality Index (WQI)	Dissolved Oxygen	0.35	In-situ measurements from water monitoring sites
	Nitrogen Concentration	0.25	In-situ measurements from water monitoring sites
	Phosphorus Concentration	0.25	In-situ measurements from water monitoring sites
	Transparency	0.15	In-situ measurements from water monitoring sites
Vegetation Coverage Index (VCI)	Annual Mean NDVI	0.60	Satellite remote sensing images and multispectral inversion data
	Seasonal Variation Amplitude	0.40	Satellite remote sensing images and multispectral inversion data

Repair and improve path output

The optimized configuration plan is spatially mapped according to the plot-level implementation unit in the output stage to form a directly executable path file for rural ecological environment restoration and ecosystem service function improvement. Based on the results of the multi-objective optimization module, the crop planting structure, farmland biodiversity configuration and water and fertilizer control parameters are allocated to each plot unit in the experimental area. The mapping process is based on the spatial overlay analysis of the geographic information system (GIS). $\mathbf{X}=[x_{ij}]$. The spatial vector data of the plots are in one-to-one correspondence, where x_{ij}represents the optimal value of the management variable for i the th plot j. The management variables include crop planting ratio, vegetation type configuration index, and water and fertilizer management parameters.

For soil quality restoration, the annual soil improvement amount is calculated based on the difference between the target value S_{target} and the current value of S_{current} soil organic matter improvement A_{soil} as follows:

$$A_{\text{soil}}=\frac{(S_{\text{target}}-S_{\text{current}})\cdot\rho_{\text{soil}}\cdot d_{\text{till}}\cdot A_{\text{plot}}}{C_{\text{amend}}} \quad \text{(Eq.7)}$$

where, ρ_{soil} is the soil density of the cultivated layer ($kg\cdot m^{-3}$), d_{till} is the tillage depth (m), A_{plot} is the plot area (m^2), C_{amend} is the organic matter content ratio of the amendment.

The water body restoration plan is based on the difference between the water quality comprehensive index improvement target W_{target} and the predicted value W_{pred}. The

http://www.aloki.hu ● ISSN 1589 1623 (Print) ● ISSN1785 0037 (Online)
DOI: http://dx.doi.org/10.15666/aeer/2401_611633

amount of ecological restoration materials to be added is determined M_{water} by the following formula:

$$M_{water}=\frac{(W_{target}-W_{pred})\cdot V_{water}}{E_{unit}} \quad \text{(Eq.8)}$$

Among them, V_{water} is the target water volume (m3^3), E_{unit} and is the unit improvement effect of the remediation material on the water quality index.

The vegetation coverage improvement path is based on the target coverage V_{target} and the current predicted value V_{pred}, combined with the plot vegetation growth potential index P_{veg}, and the planting density of the required new vegetation is calculated D_{veg} according to the following formula:

$$D_{veg}=\frac{(V_{target}-V_{pred})\cdot A_{plot}}{P_{veg}} \quad \text{(Eq.9)}$$

Among them, A_{plot} is the area of the implementation plot (m^2).

The above restoration and improvement targets are converted into an annual work plan, forming an annual restoration and improvement matrix $\mathbf{Y}=[y_{ik}]$, where y_{ik}represents the restoration workload required for i the plot in k year . Once generated, the matrix is used to schedule operations based on the agricultural production cycle, ensuring that water restoration, soil improvement, and vegetation restoration do not interfere with each other's seasonal rhythms. The final path file is output as both a table and a spatial graph. The table records the restoration tasks and parameter values for each plot in each year, while the spatial graph labels the corresponding management measures based on plot boundaries, achieving a precise mapping from optimization results to implementation paths.

Overview of the experimental area and data acquisition

The experiment area is situated in a typical northern temperate agroecological zone, ranging in coordinates from 122°15′ to 122°48′ east longitude and 37°05′ to 37°42′ north latitude. The administrative area is 462.7 km², with average annual precipitation of 612 mm and average annual temperature of 11.8°C. The two soil types are primarily that of fluvo-aquic soil and cinnamon soil, with a texture of 48.2% silt, 32.6% sand and 19.2% clay. The major crops are winter wheat and summer corn with a multiple cropping index of 190%. Irrigation water is derived from the regional river network and groundwater system.

This article utilized three types of core data: remote sensing time series, ground monitoring data, and agricultural management data. This data provided a comprehensive foundation for model building and optimization. Remote sensing time series data includes Sentinel-2 MSI satellite images and UAV multispectral data, and years were used to build multi-year remote sensing time series data that can retrieve key information at both macro- and fine-scale spatiotemporal characteristics of the ecological environment. Ground monitoring data included data from 46 soil sampling points, 12 water quality monitoring points, and a HOBO weather station. The water quality monitoring points included farmland irrigation and drainage ditches and riverbanks and provided monitoring indicators for COD, TN, TP, and DO. Agricultural production management data were included as agricultural department records at a local level, which provided

http://www.aloki.hu ● ISSN 1589 1623 (Print) ● ISSN1785 0037 (Online)
DOI: http://dx.doi.org/10.15666/aeer/2401_611633

information such as crop types and dates, fertilizer application rates, irrigation rates, and pest/disease control methods.

Soil organic matter (SOC) was determined using the potassium dichromate external heating method, and the calculation formula is:

$$SOC=\frac{(V_0-V)\times C\times 0.003\times 1.33}{m} \quad \text{(Eq.10)}$$

wherein, $mol\cdot L^{-1}$ is the blank titration volume (mL), VVV is the sample titration volume (mL), C is the concentration of potassium dichromate solution ( ), 0.003 is $mol\cdot L^{-1}$ the mass of carbon corresponding to m0.1 ml of potassium dichromate solution (g), 1.33 is the recovery coefficient, $mol\cdot L^{-1}$ and is the mass of the air-dried soil sample (g).

VCI is calculated based on the Normalized Difference Vegetation Index (NDVI). The expression of NDVI is:

$$NDVI=\frac{\rho_{NIR}-\rho_{RED}}{\rho_{NIR}+\rho_{RED}} \quad \text{(Eq.11)}$$

Among them, ρ_{NIR} is the reflectivity in the near-infrared band, ρ_{RED} is the reflectance of the red light band. VCI is calculated based on the minimum and maximum values of NDVI:

$$VCI=\frac{NDVI-NDVI_{min}}{NDVI_{max}-NDVI_{min}} \quad \text{(Eq.12)}$$

Among them, $NDVI_{min}$ and DVI_{max} represent the minimum and maximum NDVI values of the study area in the time series, respectively.

WQI is calculated using the weighted normalization method, and the formula is:

$$WQI=\frac{\sum_{i=1}^{n} w_i q_i}{\sum_{i=1}^{n} w_i} \quad \text{(Eq.13)}$$

where, w_i is i the weight of the water quality indicator, q_i is i the quality score of the indicator, n and is the total number of indicators. The weights of each item are determined based on the variance contribution rate extracted by principal component analysis (PCA). After acquisition, all data were uniformly time-aligned. Satellite imagery, drone imagery, and ground-truth data were projected into the WGS-84 coordinate system and spatially aligned using bilinear interpolation. The imagery data were atmospherically corrected using the dark pixel subtraction (DOS) method, and isolated noisy pixels were removed using a median filter. Ground sample data and image pixels were aligned using spatial buffer analysis to ensure geographic and spectral consistency of the training samples, providing a high-quality multidimensional input dataset for subsequent ST-CNN diagnosis.

In this research, the concepts of "spatial homogeneity division + management measure comparison" were applied to differentiate treated from untreated areas. Specifically, 12 plot groups that were spatially adjacent and showed no substantially significant difference in baseline conditions (e.g. soil type, plot area, baseline soil quality, and basic crop planting structure) were identified using GIS spatial overlay analysis based on core indicators. Within each group, there were two plots. The treated areas were the plots in

http://www.aloki.hu ● ISSN 1589 1623 (Print) ● ISSN1785 0037 (Online)
DOI: http://dx.doi.org/10.15666/aeer/2401_611633

each pair that implemented the ecological agriculture optimization measures: winter wheat—summer maize—leguminous green manure crop rotation, straw return to the field, organic fertilizer application, and more refined water and fertilizer management. The untreated areas were the control plots within each group maintaining traditional management practices, continuing local routine measures. A 10m wide buffer zone was set between the two areas to avoid water and fertilizer interaction. During the monitoring phase, the same number of sampling points were simultaneously deployed in both treated and untreated areas, and sampling and analysis were conducted at the same frequency for two consecutive years to ensure the effectiveness of data comparison.

Experimental equipment and platform

Experimental data collection and analysis were accomplished using a multispectral remote sensing system from an unmanned aerial vehicle (UAV), a satellite remote sensing data acquisition platform, a ground monitoring sensor network, and mid-to-high-end workstations. The drone used was a DJI Phantom 4 Multispectral, equipped with an integrated multispectral imaging system. The sensor bands cover blue (450–520 nm), green (520–600 nm), red (630–690 nm), red edge (730–740 nm), and near-infrared (770–810 nm), with a spatial resolution of 10 cm and a radiometric resolution of 10 bits. Satellite remote sensing imagery was sourced from Sentinel-2 MSI data, with a band resolution ranging from 10 to 20 m and a revisit period of 5 days. The images were radiometrically calibrated and atmospherically corrected before use, and then spatiotemporally aligned with the UAV data using nearest neighbor interpolation. The ground monitoring system deploys soil moisture and temperature sensors (Decagon 5TE, accuracy of ±2%), a portable multi-parameter water quality meter (Hach HQ40d, for monitoring pH, conductivity, and dissolved oxygen), and a small weather station (HOBO U30) to provide real-time correction data for remote sensing and model calculations.

Data processing and analysis were performed on a workstation equipped with an NVIDIA RTX 3080 GPU, an Intel Core i9-12900K processor (3.2 GHz, 16 cores), 64 GB of RAM, a 2 TB solid-state drive, and a 10 GB graphics card. The operating system was Ubuntu 22.04 LTS. The deep learning framework used was PyTorch 2.0, with CUDA 11.8 supporting GPU-accelerated computing. Remote sensing data preprocessing was performed using QGIS and Orfeo Toolbox. Image geometric correction was performed using a second-order polynomial geometric transformation, with control point residuals less than 0.5 pixels. Registration was based on a combination of phase correlation and SIFT feature matching.

In the ST-CNN model training, the batch size is set to 32, the initial learning rate is 0.001, the optimizer is Adam, and the loss function uses the weighted mean squared error (WMSE), which is defined as:

$$L=\frac{1}{N}\sum_{i=1}^{N} w_i\cdot(y_i-\hat{y}_i)^2 \quad \text{(Eq.14)}$$

Among them, N is the sample size, y_i is the measured value, $\hat{y}_i$ is the predicted value, $\hat{y}_i$ and is the weight coefficient. According to the contribution of different environmental factors to the comprehensive evaluation, it satisfies $\sum_{i=1}^{N} w_i=1$.

The multi-objective optimization process is implemented based on an improved genetic algorithm, and the fitness function is:

http://www.aloki.hu ● ISSN 1589 1623 (Print) ● ISSN1785 0037 (Online)
DOI: http://dx.doi.org/10.15666/aeer/2401_611633

$$F=\alpha\cdot S_{eco}-\beta\cdot R_{env}+\gamma\cdot P_{agr} \quad \text{(Eq.15)}$$

where represents the comprehensive score of ecosystem service functions, R_{env} represents the environmental risk index, P_{agr} represents the stability of agricultural output, α, β, and γ are normalized weights, satisfying. In each iteration $\alpha+\beta+\gamma=1$, S_{eco} the algorithm determines the optimal solution based on the Pareto frontier and uses the crowding distance to maintain a balanced distribution of solutions.

All computing tasks are run on the local workstation, using PyTorch's built-in DataLoader to manage data flow, and using NVIDIA Nsight Systems to monitor GPU utilization and memory usage, ensuring that model training and optimization decision-making processes are completed in a stable and controllable computing environment.

Experimental design

The overall experimental plan follows a process of "data collection - data preprocessing - model training and validation - optimized model operation - plan output," aiming to ensure the repeatability and verifiability of the path for rural ecological restoration and ecosystem service enhancement. The experiment was conducted in a representative rural agricultural region characterized by high farming intensity, diverse crop types, and significant ecological degradation.

The basic environmental parameters of the experimental area are shown in *Table 3*. This table covers core basic information such as soil type, climate characteristics, and the proportion of major crops planted. This data provides prior conditions for subsequent remote sensing image interpretation, ground sampling design, and model parameter setting.

Table 3. *Basic environmental parameters of the experimental area*

Parameter Category	Parameter Name	Value/Range	Unit
Soil Type	Dominant Type	Loam	—
Climate Feature	Annual Precipitation	612	mm
Climate Feature	Annual Mean Temperature	11.8	℃
Agricultural Structure	Wheat Planting Area Ratio	42	%
Agricultural Structure	Maize Planting Area Ratio	38	%
Agricultural Structure	Rapeseed Planting Area Ratio	12	%
Agricultural Structure	Other Crops Ratio	8	%

Data collection is accomplished collaboratively across multiple platforms, including drone multispectral remote sensing systems, satellite remote sensing data, ground-based soil and water quality monitoring systems, and meteorological observation equipment. Data collection spans all seasons, capturing the full temporal sequence of crop growth cycles and ecological changes. In terms of spatial coverage, remote sensing data and ground monitoring points form a multi-scale spatial resolution system, achieving vertical resolution coupling from 0.10 m at the plot level to 20 m at the regional level.

http://www.aloki.hu ● ISSN 1589 1623 (Print) ● ISSN1785 0037 (Online)
DOI: http://dx.doi.org/10.15666/aeer/2401_611633

Results

Analysis of soil quality improvement effects

To monitor the improvement of soil quality in the experimental area, this study obtained multi-period data on organic matter, pH, total nitrogen, available phosphorus, and available potassium based on seasonal sampling and analysis from 2022 to 2023. Time series matching and cross-validation were performed in combination with the inversion results of drone multispectral images and ground-based measured data to ensure the spatial and temporal consistency of the data. The monitoring cycle was set to once a quarter, covering the critical period of crop growth and the high-frequency stage of agricultural activities, thereby reflecting the dynamic changes in soil physical and chemical properties under different management and natural conditions. This study adjusted the cropping system based on the existing double-cropping system of winter wheat and summer maize in the experimental area, and optimized it by introducing a rotation pattern of winter wheat, summer maize, and leguminous green manure. Leguminous green manure was planted on 35% of the cultivated land in the experimental area, and was sown after the summer maize harvest each year and plowed into the field before the wheat sowing the following year, achieving a combination of soil conservation and land use. Differentiated application rates were implemented for winter wheat and summer maize: 6.0 t/hm² for winter wheat and 8.5 t/hm² for summer maize. The application covered all cultivated land in the experimental area, using a mechanical plowing method after crushing, directly related to the improvement of soil organic matter. Well-rotted livestock and poultry manure was used as organic fertilizer, replacing 30% of the chemical nitrogen, phosphorus, and potassium nutrient input, applied 10 days before wheat and maize sowing. After being evenly spread, the fertilizer was rotary tilled into the soil, covering all cultivated land in the experimental area. Combined with optimized irrigation to reduce nutrient loss, the soil pH was synergistically regulated through leguminous green manure rotation and organic fertilizer to alleviate soil acidification.

After the data was corrected for radiation and atmosphere and noise was suppressed, the broken line trend analysis method was used to draw the organic matter change curve, pH change curve, and nutrient change curve, respectively, in order to show the temporal changes in soil quality indicators during the implementation of the restoration measures, as shown in *Figure 3*.

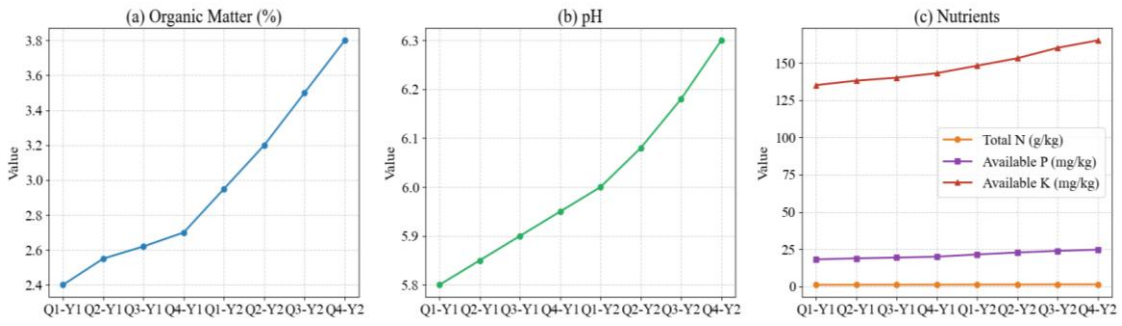

Figure 3. *Time series changes in soil quality improvement. (a) Trend of organic matter changes, (b) pH change trend, (c) Nutrient change trend*

http://www.aloki.hu ● ISSN 1589 1623 (Print) ● ISSN1785 0037 (Online)
DOI: http://dx.doi.org/10.15666/aeer/2401_611633

The data in the figure show that organic matter content increased from 2.40% in the first quarter of the first year to 3.80% in the fourth quarter of the second year. This steady growth is closely related to the long-term effects of returning straw to the fields and replacing chemical fertilizers with organic fertilizers. The pH value increased from 5.80 to 6.30, primarily due to lime acidification and appropriate crop rotation that reduced soil acidification. Total nitrogen increased from 1.15 g/kg to 1.45 g/kg, available phosphorus from 18.2 mg/kg to 24.7 mg/kg, and available potassium from 135 mg/kg to 165 mg/kg. This series of nutrient increases is closely related to the application of organic fertilizers, which increased the soil's slow-release nutrient supply capacity, and optimized irrigation, which reduced nutrient loss. The continued improvement in these indicators indicates that soil quality is steadily improving, which is conducive to the long-term and stable implementation of the subsequent ecological agriculture layout.

Analysis of vegetation coverage changes

In analyzing vegetation cover changes, we conducted a time-series monitoring of annual cover before and after the optimization plan was implemented. The seasonal changes in vegetation are based on the climate and crop rotation patterns of the northern temperate agroecological zone, and are divided into the “growing season” (April-October) and the “non-growing season” (November-March of the following year) by combining monthly time-series data from NDVI. Within the growing season, the changes are further subdivided into three subtypes according to crop phenology: “crop greening-jointing stage” in April-May, “vigorous growth stage” in June-August, and “maturity-harvest stage” in September-October. The non-growing season is divided into “bare land fallow type” and “covered crop type” according to the mulch management measures. Combining multi-source remote sensing data with drone multispectral imagery, we generated a monthly series of vegetation index changes. High-precision registration and atmospheric correction techniques were used to eliminate systematic biases in the data collection process, ensuring the authenticity and comparability of seasonal trends. We then compared and analyzed the cover curves under the two management models, and calculated the monthly improvement series to reveal the seasonal vegetation improvement characteristics of the optimized eco-agricultural layout. The results are shown in *Figure 4*.

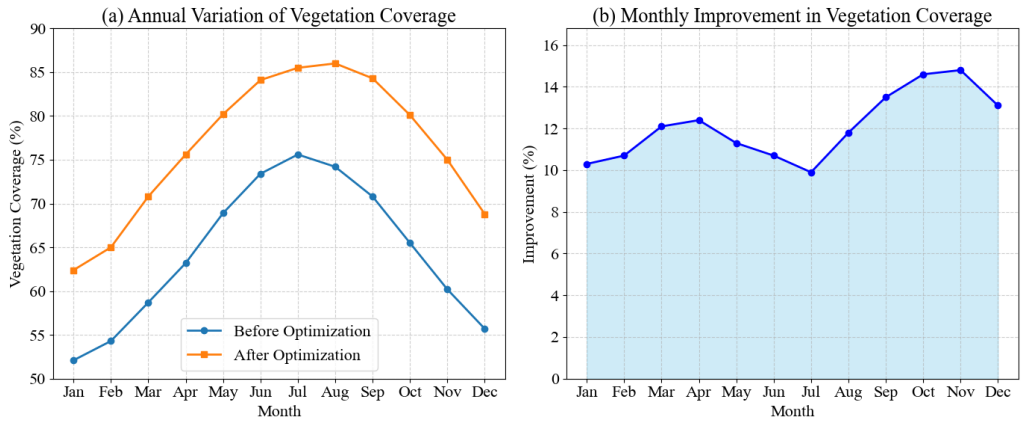

Figure 4. *Trends in vegetation coverage changes and improvements. (a) Annual trends in vegetation coverage, (b) Monthly trends in vegetation coverage improvements*

http://www.aloki.hu ● ISSN 1589 1623 (Print) ● ISSN1785 0037 (Online)
DOI: http://dx.doi.org/10.15666/aeer/2401_611633

Under the optimized plan, vegetation cover remained above 75% from April to August, reaching 86.0% in August. This represents a significant difference from the 74.2% achieved under unoptimized conditions during the same period. This is primarily due to the optimized layout increasing the proportion of crops with high growth periods and improving water and fertilizer conditions, thereby prolonging the maintenance of high cover. In November and December, the off-season months, the improvements reached 14.8% and 13.1%, respectively, exceeding the growth season differences. This is due to the increased allocation of cover crops to fallow fields during winter, which reduced the proportion of bare land and, in turn, boosted the winter vegetation index. The improvement ranged from 9.9% to 14.8% throughout the year, reflecting the combined effects of farmland management measures and seasonal vegetation growth patterns, indicating that the optimization measures consistently improved cover throughout the year.

Analysis of changes in comprehensive water quality index

In this experiment, we conducted a comprehensive analysis of changes in rural water quality across different temporal and spatial scales before and after restoration, using monthly water quality index (WQI) time-series data, key parameter measurements, and improvement assessments from multiple monitoring sites. High-resolution water quality data were simultaneously obtained through drone-based multispectral imagery and ground-based monitoring stations. Combined with laboratory analyses, quantitative indicators of dissolved oxygen, chemical oxygen demand, and total nitrogen were generated to construct a multidimensional dataset characterizing water quality dynamics. During data processing, three aspects—temporal variation, parameter composition, and spatial distribution—were normalized and visualized to elucidate the characteristics of water quality improvement across time, parameters, and spatial locations. The results are presented in *Figure 5*.

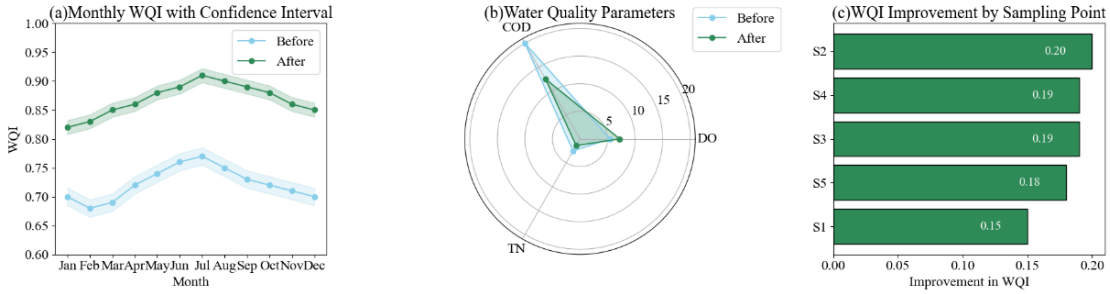

Figure 5. *Time series changes of comprehensive water quality index and parameter improvement analysis. (a) Monthly scale water quality comprehensive index change diagram, (b) Radar chart of main water quality parameters, (c) Improvement of water quality comprehensive index at the same sampling point*

Experimental results indicate that the comprehensive water quality index exhibited an overall upward trend following the implementation of the restoration measures, reaching a maximum of 0.91 and a minimum of 0.82, with markedly reduced fluctuations. This improvement is attributed to the reduction of non-point source pollution during the rainy season and the enhanced self-purification capacity of the water body. Dissolved oxygen levels increased from 5.5 mg/L to 7.2 mg/L, primarily due to the restoration of aquatic

http://www.aloki.hu ● ISSN 1589 1623 (Print) ● ISSN1785 0037 (Online)
DOI: http://dx.doi.org/10.15666/aeer/2401_611633

vegetation and improved hydrodynamics. Chemical oxygen demand decreased from 20.0 mg/L to 12.5 mg/L, reflecting enhanced degradation efficiency of organic pollutants. Total nitrogen concentrations declined from 2.5 mg/L to 1.4 mg/L, largely resulting from the reduction of non-point agricultural nitrogen inputs. Improvements ranged from 0.15 to 0.20 across all sampling sites, with the most significant enhancement observed at site S2, likely due to its proximity to major treatment facilities and the higher frequency of water exchange. Overall, the spatial consistency of water quality improvements and the emergence of localized high-improvement zones suggest that the implemented treatment measures have achieved stable and sustained enhancements over both temporal and spatial dimensions.

Analysis of changes in ecosystem service function scores

In this phase of the study, we systematically monitored and quantitatively evaluated the multidimensional characteristics of ecosystem service functions within the experimental area. By integrating drone-based multispectral imagery, remote sensing observations, and ground-based measurement data, we calculated functional scores for provisioning, regulating, supporting, and cultural services. A comprehensive analytical framework was established to assess proportional structure, functional improvements, and average scores, visualizing the spatial distribution and temporal variations of these service functions through multiple graphical representations. To ensure multidimensional evaluation, radar charts were used to display the distribution of multiple functional indicators, stacked bar charts to illustrate the proportional composition of different service types, line charts to present functional improvements over time, and ring charts to depict the overall average functional score. These combined visualizations provided a holistic representation of changes in ecosystem service functions in the experimental area before and after restoration, as shown in *Figure 6*.

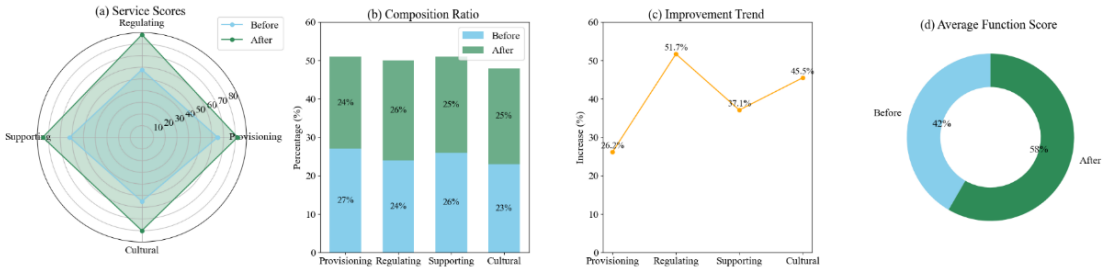

Figure 6. *Multidimensional analysis of changes in ecosystem service functions. (a) Radar chart of various service functions, (b) Stacked chart of service function composition, (c) Line chart of function improvement, (d) Average functional score ring plot*

The supply services score in the experimental area increased from 65 before restoration to 82 after restoration. Regulating services rose from 58 to 88, supporting services from 62 to 85, and cultural services from 55 to 80. This overall improvement is closely associated with the synergistic effects of crop layout optimization, vegetation restoration, and integrated soil and water management measures implemented during the restoration process. In terms of composition, regulating services accounted for 26% after restoration, up from 24% before restoration, reflecting improvements in water purification and microclimate regulation. The proportion of supply services decreased to 24%,

http://www.aloki.hu ● ISSN 1589 1623 (Print) ● ISSN1785 0037 (Online)
DOI: http://dx.doi.org/10.15666/aeer/2401_611633

corresponding to adjustments in crop structure and enhanced biodiversity allocation. Among the functional categories, regulating services increased by 51.7% and cultural services by 45.5%, directly linked to rural landscape restoration and the enhancement of ecotourism potential. The overall average functional score increased from 60 to 84, indicating a significant improvement in the comprehensive benefits of eco-agricultural measures across multiple ecological functions.

Analysis of the synergistic benefits of agricultural production and ecology

In a joint analysis of agricultural production and ecosystem function enhancement, multi-source monitoring data were used to match the output stability of each plot with the degree of improvement in ecosystem service functions. A quadratic polynomial fitting method was employed to characterize the relationship between these two variables. A boxplot of output stability distribution was constructed according to ecological improvement intervals to reveal variations in agricultural production stability under different levels of ecological enhancement. The relationship between ecological improvement and output stability, derived through curve fitting and statistical analysis of the data distribution within each improvement interval, is illustrated in *Figure 7*.

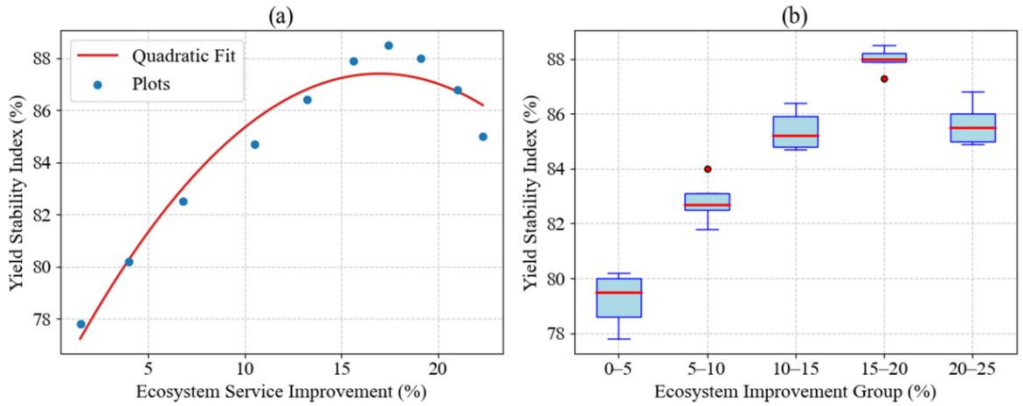

Figure 7. *Analysis of the relationship between agricultural production stability and ecological improvement. (a) Quadratic fitting curve of output stability and ecological improvement, (b) Output stability distribution in different ecological improvement intervals*

Within the ecological improvement range of 1.5% to 17.4%, yield stability increased from 77.8% to 88.5%. This upward trend is closely related to the improved soil structure, enhanced water retention capacity, and improved crop stress tolerance brought about by low- to medium-level ecological improvements. When ecological improvement continued to increase to 22.3%, yield stability decreased to 85.0%, primarily due to mismatched water and fertilizer regulation and excessive adjustments in community structure during the high-level ecological intervention phase, which increased yield fluctuations in some high-yield crops. A boxplot of the ecological improvement intervals shows that the median yield stability reached 88.0% within the 15–20% range, with a relatively small fluctuation range, reflecting the relatively stable overall benefits of management measures in this interval. Overall, the relationship between yield stability and ecological improvement shows an initial upward trend followed by a downward trend. In the high-level improvement interval, further optimization of management strategies to align inputs with crop structure is needed.

http://www.aloki.hu ● ISSN 1589 1623 (Print) ● ISSN1785 0037 (Online)
DOI: http://dx.doi.org/10.15666/aeer/2401_611633

Discussion

The substantial enhancement in soil quality demonstrated in this study—represented by increases in soil organic matter (SOM) from 2.40% to 3.80%, pH from 5.80 to 6.30, total nitrogen from 0.167% to 0.210%, available phosphorus from 14.44 mg/kg to 19.59 mg/kg, and available potassium from 139.1 mg/kg to 162.0 mg/kg, representing increases of 26.1%, 35.7%, and 22.2%, respectively—is attributable to the synergistic effects of strategic agronomic adaptations and ecological management. First, using a combination of straw return alongside organic fertilizer (15 t/hm²) provided direct increases to carbon and nutrient inputs to the soil: straw decomposition by soil microbial communities promoted SOM, while organic fertilizer served as a slow-release nutrient source and reduced nutrient leaching, addressing the nutrient deficiencies left by long-term conventional chemical fertilization. Secondly, incorporating leguminous green manure into the “winter wheat–summer maize” cropping rotation system buffered soil pH through increased concentrations of base cations and counteracted soil acidification resulting from dramatic increases in nitrogen fertilizer. The ST-CNN model dynamic monitoring of the treatment further supported the findings that the agronomic management adjustments were sustainable across seasons—SOM was consistently increasing (Q1-Y1 to Q4-Y2) with no seasonal fluctuations exceeding 5%, which indicates a lasting improvement in soil quality under optimized management.

The simultaneous improvement in both vegetation cover and water quality illustrates the relationship between regulation of the terrestrial and aquatic ecosystem in the study site. Vegetation cover reached 86.0% in August and 65.0% or greater during the non-growing season, as a result of two interventions: improved crop planting structure and planting of winter cover crops in fallowed fields, which reduced soil area by 40% in fallowed fields. Not only did the additional vegetation cover contribute to photosynthetic carbon sequestration but the vegetation also acted as a physical filter for surface runoff, leading to less nitrogen and phosphorus to water bodies. Similarly, the overall WQI reached a maximum of 0.91, with dissolved oxygen increasing from 5.5 to 7.2 $mg \cdot L^{-1}$ due to decreased non-point source pollution and increased aquatic vegetation in irrigation ditches. Vegetation-water interactions such as these underscore the importance of ecological connectivity at the landscape scale in improving water quality, providing a direct link to the "terrestrial–aquatic coordination," a concept identified in the multi-objective optimization framework.

The remarkable rise in ecosystem service scores—from 60 to 84 for the composite index, with regulating services increasing by 51.7% and cultural services by 45.5%—demonstrates the advancement toward integrating production and ecological objectives through the optimization of this study. Regulating services benefitted the greatest from improved soil and water quality: since SOM content improved, the soil's capacity for water retention also improved. Additionally, since nutrient runoff reduced the potential for eutrophication in surrounding water, and overall, there was an increase in the ecosystem's ability to regulate the microclimate and cleanse pollution. Cultural services were increased due to the diversified landscape, which provided opportunity for the aesthetic experience and ecotourism potential—an upscale experience typically left out of consideration in agricultural systems. While it was surprising to see a slight reduction in the provision of services, yield stability remained above 85%, illustrating that the rank-based multi-objective optimization algorithm could use tradeoffs to achieve a mix of ecological benefits while maintaining production security along the pareto frontier.

http://www.aloki.hu ● ISSN 1589 1623 (Print) ● ISSN1785 0037 (Online)
DOI: http://dx.doi.org/10.15666/aeer/2401_611633

The connection between ecological improvement and agricultural production stability—initially rising then slightly decreased—profoundly informs practical management implications in intensive agricultural regions. Ecological improvement of 1.5% to 17.4% was associated with enhancing yield stability of 77.8% to 88.5% as soil structure improved and crops had more resistance to stress. However, beyond 17.4% of ecological improvement, yield stability declined to 85.0% due to over-correcting crop structure as excessive cover crop biomass was competing with cash crops for sunlight, and nutrients. This threshold effect demonstrates that the ecological management of intensive agricultural systems relies on "moderating" ecological principles, and was not successful in maintaining production stability after high-intensity ecological improvements could not account for local variations in requirements for cash crop growth. The 15–20% ecological improvement range, during which yield stability peaked and fluctuations were minimal, can serve as a practical guide for management in similar temperate agroecological zones.

Overall, these findings confirm the study's comprehensive "monitoring–diagnosis–optimization" framework targeting rural ecological degradation. The ST-CNN model integrates satellite/UAV remote sensing and in situ data, allowing real-time monitoring of soil–water–vegetation dynamics that the previous approach lacked, while the multi-objective optimization algorithm was able to avoid the trade-offs of single criterion planning (the traditional way of managing agriculture has been to maximize yield, often at the expense of ecological consideration). The framework provides a transferable monitoring and optimization tool for data-sparse rural areas of China where traditional management priorities have favored yields over ecology, and it is advanced through the incorporation of basic remote sensing data and periodic ground sampling, thus minimizing dependence on large- cost long-term monitoring networks. There is significant scope for applications of these methods to enhance this framework by adding local crop varieties and climate conditions, which will ensure optimal usability and fit in diverse agroecological contexts.

Conclusion

Confronting rural ecological degradation and declining ecosystem services, this study developed an integrated, closed-loop restoration pathway that couples monitoring–diagnosis–optimization–implementation. We fused satellite remote sensing, UAV multispectral imagery, and multi-source environmental and management records to construct a spatiotemporal convolutional neural network (ST-CNN) for dynamic ecological diagnosis. The model predicted soil quality index (SQI), water quality index (WQI), and vegetation cover index (VCI) by extracting multi-scale spatial–temporal features, and informed a multi-objective optimization of crop-planting structure, on-farm biodiversity allocation, and water–fertilizer management to balance ecosystem benefits with production stability.

Across the case landscape, soil organic matter increased from 2.40% to 3.80%, WQI peaked at 0.91, dissolved oxygen rose from 5.5 to 7.2 mg L^{-1}, and peak-season vegetation cover reached 86.0% in August, an 11.8-percentage-point gain over unoptimized management. The ecosystem-service composite score improved from 60 to 84. These outcomes indicate that quantitatively linking fine-scale monitoring with spatiotemporal learning and Pareto-based optimization can simultaneously reduce environmental risks,

http://www.aloki.hu ● ISSN 1589 1623 (Print) ● ISSN1785 0037 (Online)
DOI: http://dx.doi.org/10.15666/aeer/2401_611633

enhance regulating/supporting services, and stabilize agricultural outputs under ecological-agriculture regimes.

The proposed workflow provides a transferable decision-support framework for precision rural restoration, enabling indicator harmonization, spatial targeting of interventions, and adaptive scheduling of water–nutrient inputs and biodiversity management within routine management cycles to operationalize ecosystem-service objectives alongside production goals. While the outcomes are promising, broader cross-regional validation, multi-year and seasonal robustness testing, and cost–benefit analyses are required to support generalized deployment. Future research should integrate causal inference and uncertainty quantification, expand biodiversity metrics beyond vegetation cover (e.g., functional or trait diversity), and link biophysical improvements with socio-economic outcomes such as livelihoods and input efficiency. Enhancing model interpretability and developing field-scale decision tools will further strengthen its applicability and adoption in data-limited rural regions.

Funding. This research received no external funding.

Data availability statement. Data supporting the findings of this study are available from the author upon reasonable request.

Conflicts of interest. The author declares no conflict of interest.

REFERENCES

[1] Bai, J., Qin, Y., Zhao, J., Song, Y. (2025): Investigation of agricultural nutrient removal by ecological ditches using meta-analysis. – Agriculture, Ecosystems & Environment 380: 109401. DOI: https://doi.org/10.1016/j.agee.2024.109401.

[2] Bai, T., Yang, J., Wang, X., Su, R., Cushman, S. A., Lawson, G., Liu, M., Wang, G., Li, D., Wang, J., Zhang, J., Wu, Y. (2025): Multi-source data-driven spatiotemporal study on integrated ecosystem service value for sustainable ecosystem management in Lake Dianchi Basin. – Sustainability 17(9): 3832. DOI: https://doi.org/10.3390/su17093832.

[3] Colombi, G., Martani, E., Fornara, D. (2025): Regenerative organic agriculture and soil ecosystem service delivery: A literature review. – Ecosystem Services 73: 101721. DOI: https://doi.org/10.1016/j.ecoser.2025.101721.

[4] Gao, D. (2024): Study on the coupling coordination and barrier factors between agroecological security and rural green development in China. – Scientific Reports 14(1): 29767. DOI: https://doi.org/10.1038/s41598-024-80669-8.

[5] Gu, B., Zhang, X., Lam, S. K., Yu, Y., Van Grinsven, H. J., Zhang, S., Wang, X. X., Bodirsky, B. L., Wang, S. T., Duan, J. K., Ren, C. C., Bouwman, L., de Vries, W., Xu, J. M., Sutton, M. A., Chen, D. (2023): Cost-effective mitigation of nitrogen pollution from global croplands. – Nature 613(7942): 77-84. DOI: https://doi.org/10.1038/s41586-022-05481-8.

[6] Juncal, M. J. L., Masino, P., Bertone, E., Stewart, R. A. (2023): Towards nutrient neutrality: A review of agricultural runoff mitigation strategies and the development of a decision-making framework. – Science of the Total Environment 874: 162408. DOI: https://doi.org/10.1016/j.scitotenv.2023.162408.

[7] Kabir, E., Kim, K. H., Kwon, E. E. (2023): Biochar as a tool for the improvement of soil and environment. – Frontiers in Environmental Science 11: 1324533. DOI: https://doi.org/10.3389/fenvs.2023.1324533.

http://www.aloki.hu ● ISSN 1589 1623 (Print) ● ISSN1785 0037 (Online)
DOI: http://dx.doi.org/10.15666/aeer/2401_611633

[8] Kaur, M., Li, J., Zhang, P., Yang, H. F., Wang, L., Xu, M. (2022): Agricultural soil physico-chemical parameters and microbial abundance and diversity under long-run farming practices: A greenhouse study. – Frontiers in Ecology and Evolution 10: 1026771. DOI: https://doi.org/10.3389/fevo.2022.1026771.
[9] Knapp, J., Sciarretta, A. (2023): Agroecology: protecting, restoring, and promoting biodiversity. – BMC Ecology and Evolution 23(1): 29. DOI: https://doi.org/10.1186/s12862-023-02140-y.
[10] Lenton, T. M., Abrams, J. F., Bartsch, A., et al. (2024): Remotely sensing potential climate change tipping points across scales. – Nature Communications 15(1): 343. DOI: https://doi.org/10.1038/s41467-023-44609-w.
[11] Lewandowski, A. M., Cates, A. (2023): Connecting soil health and water quality in agricultural landscapes. – Journal of Environmental Quality 52(3): 412-421. DOI: https://doi.org/10.1002/jeq2.20390.
[12] Liu, J., Du, J., Zhang, C., Zhang, J., Yang, H., Donald, M. L., Wum Y., Dong, T. (2023): Ecosystem service assessment under ecological restoration programs: A systematic review of studies from China. – Frontiers in Ecology and Evolution 11: 1152907. DOI: https://doi.org/10.3389/fevo.2023.1152907.
[13] Lottering, R., Peerbhay, K., Adelabu, S. (2025): Remote Sensing Applications in Agricultural, Earth and Environmental Sciences. – Applied Sciences 15(8): 4537. DOI: https://doi.org/10.3390/app15084537.
[14] Madjar, R. M., Vasile Scăețeanu, G., Sandu, M. A. (2024): Nutrient water pollution from unsustainable patterns of agricultural systems, effects and measures of integrated farming. – Water 16(21): 3146. DOI: https://doi.org/10.3390/w16213146.
[15] Maes, S. L., Perring, M. P., Cohen, R., et al. (2024): Explore before you restore: Incorporating complex systems thinking in ecosystem restoration. – Journal of Applied Ecology 61(5): 922-939. DOI: https://doi.org/10.1111/1365-2664.14614.
[16] Masenyama, A., Mutanga, O., Dube, T., Bangira, T., Sibanda, M., Mabhaudhi, T. (2022): A systematic review on the use of remote sensing technologies in quantifying grasslands ecosystem services. – GIScience & Remote Sensing 59(1): 1000-1025. DOI: https://doi.org/10.1080/15481603.2022.2088652.
[17] Mehmood, M., Shahzad, A., Zafar, B., Shabbir, A., Ali, N. (2022): Remote sensing image classification: A comprehensive review and applications. – Mathematical Problems in Engineering 2022(1): 5880959. DOI: https://doi.org/10.1155/2022/5880959.
[18] Morizet-Davis, J., Marting Vidaurre, N. A., Reinmuth, E., Rezaei-Chiyaneh, E., Schlecht, V., Schmidt, S., Singh, K., Vargas-Carpintero, R., Wagner, M., von Cossel, M. (2023): Ecosystem services at the farm level—Overview, synergies, trade-offs, and stakeholder analysis. – Global Challenges 7(7): 2200225. DOI: https://doi.org/10.1002/gch2.202200225.
[19] Petrosillo, I., Valente, D., Scavuzzo, C. M., Selvan, T. (2023): Land degradation pattern and ecosystem services. – Frontiers in Environmental Science 11: 1137768. DOI: https://doi.org/10.3389/fenvs.2023.1137768.
[20] Pfeifer, M., Sallu, S. M., Marshall, A. R., et al. (2023): A systems approach framework for evaluating tree restoration interventions for social and ecological outcomes in rural tropical landscapes. – Philosophical Transactions of the Royal Society B 378(1867). DOI: https://doi.org/10.1098/rstb.2021.0111.
[21] Piczak, M. L., Robichaud, J. A., Morrison, P., Rous, A. M., Mulder, I. M., Hill, C. J., Prystay, T. S., Rosner-Katz, H., Robinson, K. F., Bennett, J. R., Cooke, S. J. (2024): Structured decision making remains underused in ecological restoration despite opportunities. – Environment Systems and Decisions 44(1): 1-15. DOI: https://doi.org/10.1007/s10669-023-09940-z.
[22] Schwantes, A. M., Firkowski, C. R., Affinito, F., Rodriguez, P. S., Fortin, M. J., Gonzalez, A. (2024): Monitoring ecosystem services with essential ecosystem service variables. –

http://www.aloki.hu ● ISSN 1589 1623 (Print) ● ISSN1785 0037 (Online)
DOI: http://dx.doi.org/10.15666/aeer/2401_611633

Frontiers in Ecology and the Environment 22(8): e2792. DOI: https://doi.org/10.1002/fee.2792.

[23] Selsam, P., Bumberger, J., Wellmann, T., Pause, M., Gey, R., Borg, E., Lausch, A. (2024): Ecosystem integrity remote sensing—modelling and service tool—ESIS/Imalys. – Remote Sensing 16(7): 1139. DOI: https://doi.org/10.3390/rs16071139.

[24] Senf, C. (2022): Seeing the system from above: The use and potential of remote sensing for studying ecosystem dynamics. – Ecosystems 25(8): 1719-1737. DOI: https://doi.org/10.1007/s10021-022-00777-2.

[25] Singh, A., Gaurav, K. (2023): Deep learning and data fusion to estimate surface soil moisture from multi-sensor satellite images. – Scientific Reports 13(1): 2251. DOI: https://doi.org/10.1038/s41598-023-28939-9.

[26] Song, Q., Gao, X., Song, Y., Li, Q., Chen, Z., Li, R., Zhang, H., Cai, S. (2023): Estimation and mapping of soil texture content based on unmanned aerial vehicle hyperspectral imaging. – Scientific Reports 13(1): 14097. DOI: https://doi.org/10.1038/s41598-023-40384-2.

[27] Sutherland, G. D., Smith, J., Louise Waterhouse, F., Saunders, S. C., Paige, K. (2022): A pragmatic approach for developing landbase cumulative effects assessments with aggregated impacts crossing multiple ecological values. – Environmental Management 69(5): 1020-1034. DOI: https://doi.org/10.1007/s00267-022-01632-9.

[28] Wang, J., Zhou, F., Xie, A. (2022): The impact of integrated development of agriculture and tourism on rural ecological environment quality. – Wireless Communications and Mobile Computing 2022(1): 6113324. DOI: https://doi.org/10.1155/2022/6113324.

[29] Wang, R., Sun, Y., Zong, J., Wang, Y., Cao, X., Wang, Y., Cheng, X., Zhang, W. (2024): Remote sensing application in ecological restoration monitoring: A systematic review. – Remote Sensing 16(12): 2204. DOI: https://doi.org/10.3390/rs16122204.

[30] Yan, J., Xiong, K., Fu, Y., Yu, N., Zhang, Z., Zheng, P. (2024): Research progress on eco-product value realization and rural revitalization and its inspiration for karst desertification control: a systematic literature review between 1997 and 2023. – Frontiers in Sustainable Food Systems 8: 1420562. DOI: https://doi.org/10.3389/fsufs.2024.1420562.

[31] Zhai, Z., Jiang, M., Chen, W., Che, X. (2022): Agricultural outputs and structure adjustments: Empirical evidence based on high-impact weather. – Frontiers in Environmental Science 10: 951607. DOI: https://doi.org/10.3389/fenvs.2022.951607.

[32] Zhang, B., Shi, Y. T., Wang, S. (2022): A review on the driving mechanisms of ecosystem services change. – Journal of Resources and Ecology 13(1): 68-79. DOI: https://doi.org/10.5814/j.issn.1674-764x.2022.01.008.

http://www.aloki.hu ● ISSN 1589 1623 (Print) ● ISSN1785 0037 (Online)
DOI: http://dx.doi.org/10.15666/aeer/2401_611633